Identification and characterization of optical and X-ray Supernova Remnants

Author: Pol Musté Ferré, pmustefe25@alumnes.ub.edu
Facultat de Física, Universitat de Barcelona, Diagonal 645, 08028 Barcelona, Spain.

Advisors: Maria Kopsacheili and Konstantina Anastasopoulou

Abstract: This paper presents a multi-wavelength analysis of supernova remnants (SNRs) in the galaxies NGC 5068 and NGC 628, based on archival optical data from MUSE and X-ray observations from *Chandra*. SNR candidates are identified through emission-line diagnostics and the selection is performed by established criteria. Extinction-corrected fluxes allow the derivation of luminosities, densities, and shock velocities. Using the optical data, a comparison between the two galaxies is carried out to identify any trends. Additionally, the X-ray counterparts of the optical candidate SNRs are identified and their properties are presented.
Keywords: ISM: supernova remnants — line: identification — galaxies: individual: NGC 5068, NGC 628 — X-rays: general
SDGs: Quality education

I. INTRODUCTION

Supernova remnants (SNRs) are the expanding structures left behind after the explosive death of massive stars. These remnants originate when a supernova injects a tremendous amount of energy into the surrounding interstellar medium (ISM), propelling stellar material outward in an expanding shell. The evolution of this shell is governed by its interaction with the ISM, leading to complex structures shaped by both the initial explosion parameters and the ambient environment. [1]

As the shockwave propagates through the ISM, it compresses and heats the gas, producing emissions across the electromagnetic spectrum. In the optical regime, strong emission lines, such as Hα, Hβ, [O III](λ5006), [N II](λ6548), [N II](λ6583), [S II](λ6716) and [S II](λ6730), are highlighted due to ionization and shock excitation of the gas. These emissions can be used to trace shock velocities, density variations, and elemental abundances in the shell.[7] Typically, SNRs with high shock velocities (indicative of younger remnants) exhibit strong [O III] emission, while older or slower-evolving remnants may be richer in [N II] or [S II].

In our Galaxy, there are approximately 310 supernova remnants (SNRs), most of them detected in radio.[9] The most important advantage of studying Galactic SNRs is that their detailed structures can be observed, allowing the study of the physics and kinematics in different regions of the same nebula. However, because most SNRs are expected to be in the Galactic plane, a significant fraction remains undetected due to obscuration. This problem is minimized in extragalactic studies, where face-on galaxies away from the Galactic plane are usually selected. [10] Another advantage of extragalactic studies is the possibility to investigate SNR populations and their properties in different galactic environments, such as galaxies with varying star formation rates, metallicities, and morphologies.

The optical identification of SNRs has traditionally relied on the empirical [S II]/Hα ratio, with values above 0.4 distinguishing SNRs from photoionized H III regions. However, recent developments have introduced multidimensional diagnostics using multiple emission-line ratios, improving the detection of low-excitation SNRs and reducing selection biases.[8] Integral Field Spectroscopy (IFS), such as that provided by the MUSE[1] instrument, enables both spectral and spatial resolution of emission sources, facilitating more accurate classification of SNR candidates.

X-ray data from observatories like *Chandra* provide key insights into high-energy processes in supernova remnants (SNRs). Combined optical and X-ray studies not only help estimate ages but also reveal details about the circumstellar (CSM) and interstellar media (ISM). Since X-ray emission mainly arises from young SNRs and optical emission from older ones, detecting both simultaneously suggests a non-uniform or dense environment shaped by the CSM, which is created by the stellar winds of the progenitor star. Massive stars, with stronger winds, create more irregular CSM than lower-mass stars.[10] Thus, the coexistence of strong X-ray and optical emissions can indicate the explosion type and progenitor, often pointing to a core-collapse supernova.

In this project, we focus on the galaxies NGC 5068 and NGC 628. Both are nearby, star-forming spiral galaxies, making them ideal laboratories for studying SNRs in different environments. Star formation is closely linked to core-collapse supernovae, and thus to the creation of SNRs. In this study, we identified a total of 425 optical SNR candidates in NGC 628 and NGC 5068 using multiline diagnostic criteria. We then derived key physical parameters such as Hα luminosities, shock velocities, and pre-shock densities. Additionally, we analysed archival *Chandra* data to detect X-ray sources in both galaxies and found that 9 of them are spatial counterparts to the

[1] Multi Unit Spectroscopic Explorer in the VLT (Very large Telescope), of the European Southern Observatory (ESO), in Chile.

optical SNR candidates.

II. METHODOLOGY

The analysis was carried out using custom Python scripts specially developed for this project. All scripts are available in the author's public GitHub repository.[11]

A. Optical Data Analysis (MUSE)

The optical analysis in this study is based on archival data from the MUSE instrument for the nearby galaxies NGC 628 and NGC 5068. These galaxies are suitable targets due to their moderate inclination, active star formation, and high-quality multi-wavelength coverage. The main steps of the optical analysis are detailed below.

1. Data Acquisition and Preparation

For this analysis, we utilized reduced MUSE integral field data cubes retrieved from the ESO Science Archive Facility[(2)]. We directly obtained the narrow-band emission-line maps and their associated error maps for key diagnostic lines: Hα(λ6563), Hβ(λ4861), [O III](λ5006), [N II]($\lambda\lambda$6548, 6583), [S II]($\lambda\lambda$6716, 6730).

2. Source Detection and Photometry

To detect SNR candidates, we used the `SExtractor` software [2] on stacked images combining Hα, [S II], [N II] and [O III] emission-line maps. Stacking was done to enhance the S/N and ensure the inclusion of sources that appear in at least one of the key bands.

We experimented with different `SExtractor` parameters and adopted the following optimal configuration: (a) detection threshold of 1.5σ above background, (b) minimum area of 5 contiguous pixels, and (c) background mesh size of 6 pixels to account for small-scale fluctuations. This configuration allowed the robust detection of extended SNRs while minimizing false positives due to noise.

Detected sources were then inspected visually in SAOImage DS9 to remove structures that do not resemble SNRs. Photometry was performed using the `photutils` Python package, adopting circular apertures adapted for each source size and a local annular background subtraction. In these galaxies, due to the high number of sources, the background regions were defined as annuli 1 pixel wide, offset by 1.5 pixels from the source aperture.

$$F_{\rm net} = F_{\rm source} - F_{\rm bkg} \tag{1}$$

Flux uncertainties were propagated from error maps of the different emission lines. For detailed calculations, see Appendix A.

To correct the extinction, we used the Balmer decrement, assuming an intrinsic Hα/Hβ ratio of 2.86 and adopting the extinction law with $R_V = 3.1$.[3]

3. Emission-Line Diagnostics for SNR Identification

The following flux ratios are computed for each candidate, in order to apply the multiline diagnostics: [S II]($\lambda\lambda$6716, 6730)/Hα, [N II](λ6583)/Hα, and [O III](λ5007)/Hβ. The sources with a signal-to-noise ratio greater than 3 (SNR = ratio/$\sigma_{\rm ratio}$ > 3) in each emission line ratio are retained.

Five diagnostic criteria were applied:

1. The classical [S II]/Hα > 0.4 criterion, commonly used to separate SNRs from H II regions.

2. Four 2D/3D diagnostics developed by M. Kopsacheili et al.[7], involving combinations of the three line ratios. For the diagnostic functions used in this work, see Appendix B.

For this study, only sources satisfying at least three of the four multidimensional diagnostics were classified as robust optical SNR candidates.

4. Physical Parameter Estimation

We derived physical parameters from the extinction-corrected fluxes from the SNRs that passed the diagnostics:

- **Luminosities:** Luminosities were calculated using the following expression:

  $$L = 4\pi d^2 F \tag{2}$$

  where F is the flux in erg/s/cm^2 (units of the flux maps) and d is the distance to the galaxy. The adopted distances[(3)] were 8.63 ± 0.30 Mpc for NGC 628 and 5.16 ± 0.35 Mpc for NGC 5068.

- **Densities:** Estimated using the [S II](λ6716)/[S II](λ6730) ratio under the assumtion of 4 different temperatures: 5×10^3 K, 10^4 K, 3×10^4 K, 5×10^4 K. These computations were performed using the `PyNeb` package, which applies.....

- **Shock Velocities:** To compute the shock velocities of the SNRs, different 3D shock models were employed. Shock velocities were estimated from the [S II]($\lambda\lambda$6716, 6730)/Hα, [N II]($\lambda\lambda$6548, 6583)/Hα, and [O III](λ5007)/Hβ ratios using the shock model grids. [5] Based on the measured line ratios, an interpolation over these model grids was performed using the `interpolate` function from the `scipy` package in Python.

---

[2] Retrieved MUSE 3D maps: `https://www.eso.org/rm/api/v1/public/releaseDescriptions/184`

[3] Distances obtained from: `https://ned.ipac.caltech.edu/`

B. X-ray Data Analysis (*Chandra*)

The X-ray analysis was performed using archival observations from the *Chandra* X-ray Observatory for NGC 628 and NGC 5068. All data were processed with the `CIAO` software suite, following standard procedures including reprocessing, flare filtering, source detection, and cross-identification with optical SNR candidates.

1. Data retrieval and reduction

Chandra ACIS-S observations for both galaxies were downloaded from *Chandra* repository[4]. The datasets were reprocessed with the `chandra repro` script to generate new Level 2 event files (`evt2.fits`). These files contain cleaned and calibrated records of detected X-ray photon events, including energy, time, and position information. For NGC 5068, a single observation (OBSID 15385) was selected for its depth and quality. For NGC 628, two observations (OBSID 02057 and 02058) were used. We then corrected the event files of all OBSIDs for background flares, which were detected only for OBSID 02057. The final exposure times are 47.44, 40.00 and 40.00 ks for OBSIDs 15385, 16002, and 16003 respectively.

For NGC 5068 the `fluximage` tool was then used to generate exposure-corrected images and exposure maps in different energy bands (soft: 0.5–1.2 keV, medium: 1.2–2.0 keV, hard: 2.0–7.0 keV, broad: 0.5–7.0 keV).

Since the observations of NGC 628 were taken very close in time, the event files were merged with `merge_obs`, which internally creates combined images, exposure maps, and aspect solutions equivalent to the output of `fluximage`.

2. Source detection and classification

The `wavdetect` algorithm was applied to the images in each energy band. This tool uses a wavelet transform to identify significant structures at multiple spatial scales (e.g., 1, 2, 4, 8, and 16 pixels), filtering out spurious detections based on a significance threshold. Searching in all energy X-ray bands, the wavdetect algorithm resulted in 98 X-ray sources in NGC 628 and 29 X-ray sources for NGC 5068.

3. Cross-matching with the optical catalog

Detected X-ray sources were visually and positionally compared with the optical SNR candidates identified from MUSE data. Cross-matching was performed in DS9 using region overlays to identify the X-ray counterparts to the optical candidate SNRs that passed at least three multiline diagnostic criteria.

4. Joint characterization

For the number of sources detected in both optical and X-ray bands, annuli were manually defined around each source to calculate net count rates (background-subtracted) in each energy band including at least 90 per cent of the encircled energy at 1.49 keV of an on-axis point source for the ACIS-S camera. This step was done using DS9 analysis. To assess the significance of each X-ray detected source, we calculated the signal-to-noise ratio as follows:

$$\mathrm{S/N} = \frac{R_{\mathrm{net}}}{\sigma_{R_{\mathrm{net}}}} \tag{3}$$

where R_{net} is the net count rate, obtained by subtracting the background counts from the total source counts and dividing by the exposure time, and σ_{net} is the uncertainty on R_{net}, calculated assuming Gaussian statistics. The count rates were converted to absorbed and unabsorbed (i.e., corrected for Galactic absorption)[5] fluxes in the broad band using appropriate count-rate to flux conversion factors obtained from the PIMMS toolkit[6]. Finally, luminosities were calculated using the corresponding equation (2) and the known distances to each galaxy.

III. RESULTS

This section presents the results obtained from the identification and analysis of SNRs in the galaxies NGC 628 and NGC 5068 using both optical and X-ray data. The properties derived from the optical study include luminosities, densities, and shock velocities. A brief overview of the X-ray counterpart analysis is provided.

A. Number of SNRs Identified

Table I summarizes the number of supernova remnant (SNR) candidates identified in both galaxies across different diagnostics. We detected 158 and 267 optical SNRs for NGC 628 and NGC 5068, respectively. Cross-matching with *Chandra* X-ray data yielded 5 coincident sources in NGC 628 and 4 in NGC 5068. The color images of both galaxies, showing the positions of the sources identified in optical and X-ray, are provided in Appendix C.

Galaxy	Optical ($\geq$ 3 Diagnostics)	X-ray SNRs
NGC 628	158	5
NGC 5068	267	4

TABLE I: Summary of the number of SNRs in NGC 628 and NGC 5068 detected in optical and X-rays.

It is worth noting that if only the classical diagnostic criterion ([S II]/Hα $>$ 0.4) had been used, signifi-

[4] *Chandra* repository webpage: `https://cda.harvard.edu/chaser/`

[5] The N_{H} values were fixed at the weighted average value toward the center of the galaxies provided by the HEASARC tool N_H: `https://heasarc.gsfc.nasa.gov/cgi-bin/Tools/w3nh/w3nh.pl`

[6] PIMMS toolkit: `https://cxc.harvard.edu/toolkit/pimms.jsp`

cantly fewer sources would have been identified. Specifically, only 106 sources in NGC 628 and 190 sources in NGC 5068 would have satisfied this condition.

B. Luminosity Distributions

Fig. 1 shows the normalized probability distributions of the logarithmic luminosities for Hα for both galaxies. The remaining results for Hβ, [O III], [S II] and [N II] are shown in Fig. 6 in Appendix D. The distributions were modeled using Gaussian fits in log-space, with best-fit parameters obtained via a Markov Chain Monte Carlo (MCMC) sampling approach using the `emcee` Python package. A total of 100,000 iterations were performed to ensure convergence and robust error estimation.

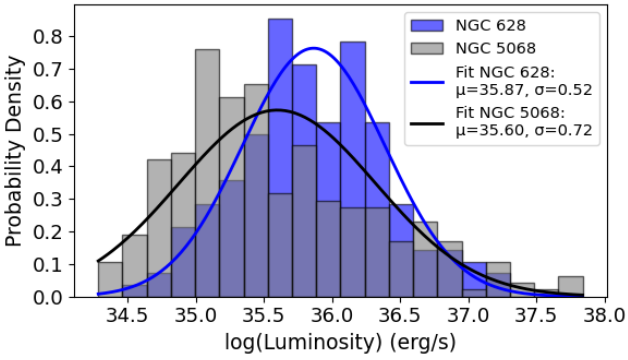

FIG. 1: Probability distributions of extinction-corrected luminosities for Hα in NGC 628 and NGC 5068.

The parameters (mean μ and standard deviation σ) of the best-fitting Gaussian models are presented in Table II.

	NGC 628		NGC 5068	
Luminosity	$\mu(\log_{10}(L))$	$\sigma(\log_{10}(L))$	$\mu(\log_{10}(L))$	$\sigma(\log_{10}(L))$
Hα	35.87	0.52	35.60	0.72
Hβ	35.25	0.52	35.00	0.75
[O III]	35.57	0.49	35.25	0.79
[S II]	35.56	0.59	35.29	0.70
[N II]	35.82	0.59	35.15	0.75

TABLE II: Best-fit Gaussian parameters (mean μ and standard deviation σ) for the $\log_{10}$-luminosities (in erg/s) of various emission lines.

C. Densities

Densities were estimated using the [S II](λ6716)/[S II](λ6730) ratio and various typical temperatures in SNRs (T = 5×10^3, 10^4, 3×10^4, and 5×10^4 K). Fig. 2 shows the density distribution for T = 10^4 K in both galaxies. The remaining temperatures are shown in Fig. 7 in Appendix E. For each temperature, the density distributions were modeled using Gaussian or skewed Gaussian profiles depending on the observed symmetry of the data. Fitting was again carried out using the `emcee` package.

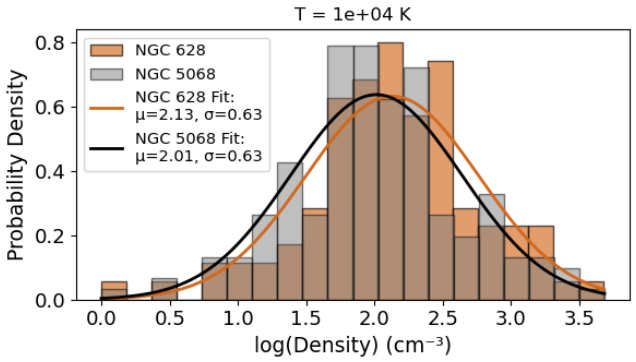

FIG. 2: Probability density functions of the estimated densities for both galaxies at a temperature of 10^4 K.

The results of the best-fit parameters are shown in Table III. The skew parameter α is omitted in cases where a standard Gaussian provided a sufficient fit.

	NGC 628			NGC 5068		
Temperature	μ	σ	α	μ	σ	α
5×10^3	2.05	0.55	-	1.95	0.57	-
1×10^4	2.13	0.63	-	2.01	0.63	-
3×10^4	2.29	0.73	-	2.20	0.74	-
5×10^4	3.28	1.18	-2.73	3.19	1.19	-2.26

TABLE III: Best-fit Gaussian parameters for the density distributions in $\log(\text{cm}^{-3})$, at various assumed temperatures. Best-fit Gaussian parameters (mean μ, standard deviation σ and skewness α) for the $\log_{10}$-densities (in cm^{-3}), at various assumed temperatures.

D. Shock Velocities

The resulting velocity distributions are shown in Fig. 3. The distributions indicate that SNRs in NGC 5068 tend to have higher shock velocities on average, suggesting the presence of younger, more energetic remnants. This correlates with higher [O III]/Hβ ratios observed in this galaxy.

Additionally, when the interpolation of measured line ratios over the models of shock velocities was applied, a small number of sources did not fit in the model. A fraction of these had an unusually high [N II]/Hα ratio that lay outside the boundaries of the 3D model. In these cases, the [N II] emission is higher than Hα emissions.

E. X-ray Properties of Confirmed SNRs

Among the optically confirmed SNRs, 5 in NGC 628 and 4 in NGC 5068 show spatial coincidence with X-ray sources. The sky coordinates, fluxes, luminosities,

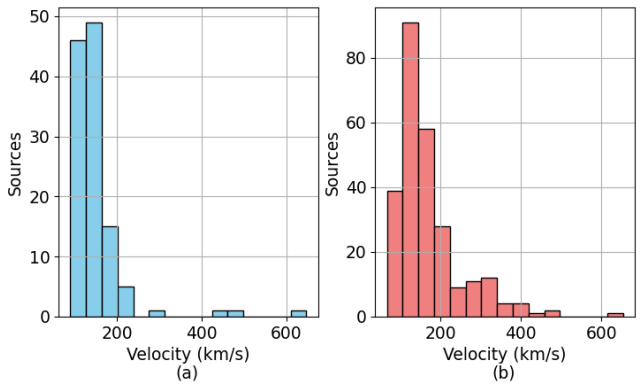

FIG. 3: Histogram of interpolated shock velocities (km/s) for confirmed SNRs in NGC 628 (a) and NGC 5068 (b).

S/N, and the additional energy bands in which each source was detected, are reported in Table IV in Appendix F. From both galaxies there are 5 strong detections (S/N>3). Out of the 9 X-ray sources, 5 predominantly show soft/medium emission.

IV. CONCLUSIONS

In this thesis, we have carried out a comprehensive multi-wavelength study of SNRs in the nearby, star-forming galaxies NGC 628 and NGC 5068. By combining optical observations from the MUSE integral field spectrograph with X-ray data from the *Chandra* X-ray Observatory, we developed and applied a robust methodology to identify and analyze the SNR populations in both systems. Our approach integrated classical line ratio diagnostics with modern, multidimensional diagnostic diagrams based on emission from [S II], [N II], [O III], Hα, and Hβ. Only sources that met at least three of the four multidimensional criteria were retained in the final catalogue, thereby significantly reducing contamination from H II regions and ensuring the robustness of the selected sample.

A total of 158 and 5 SNRs have been identified in NGC 628 in the optical and X-ray, respectively, while 267 and 4 have been found for NGC 5068. Notably, this represents the first report of X-ray SNRs in NGC 5068. In NGC 628, all X-ray SNRs are new detections. In the optical, 79 and 176 are new identifications for NGC 628 and NGC 5068, respectively.[4]

In addition to the X-ray and optical detections, the multiline information provided by integral field spectroscopy (IFS) data has been utilized to construct luminosity functions of SNRs for all the emission lines used in their detection. Furthermore, this multiline information has been combined with theory and models in order to estimate both the shock velocity and the pre-shock density.

Potential future extensions of this work include, a more in-depth comparison between the X-ray and the optical properties of SNRs, expanding the SNR sample by considering sources from both galaxies that were previously discarded for failing to meet at least three diagnostic criteria, as well as incorporating new candidates from other galaxies. With a more extensive dataset, new correlations among SNR properties may be uncovered, offering deeper insight into their evolution and the diversity of physical conditions in different galactic environments.

Acknowledgments

I want to thank my supervisors for their help and guidance during this project. I'm especially grateful to Dr. Maria Kospacheili for her support and mentorship with the optical part, and to Dr. Konstantina Anastasopoulou for her help and expertise with the X-ray analysis. Their advice and feedback were very important throughout this thesis.

[1] B. T. Draine. *Physics of the Interstellar and Intergalactic Medium*. Princeton University Press, 2011.

[2] E. Bertin. et al. Sextractor: Software for source extraction. *Astron. Astrophys. Suppl. Ser.*, 117(2):393–404, 1996.

[3] J. A. Cardelli. et al. The relationship between infrared, optical, and ultraviolet extinction. *Astrophysical Journal*, 345:245–256, 1989.

[4] J. Li. et al. Discovery of 2200 new supernova remnants in 19 nearby star-forming galaxies with muse spectroscopy. *AA*, 690:A161, 2024.

[5] M. G. Allen. et al. The mappings iii library of fast radiative shock models. *The Astrophysical Journal Supplement Series*, 178(1):20–55, September 2008.

[6] M. Kopsacheili. et al. Diagnostics-for-snr-identification. `https://github.com/mariakop21/Diagnostics-for-SNR-identification`. GitHub repository.

[7] M. Kopsacheili. et al. A diagnostic tool for the identification of supernova remnants. *Monthly Notices of the Royal Astronomical Society*, 491(1):889–902, 11 2019.

[8] M. Kopsacheili. et al. Supernova remnant properties and luminosity functions in ngc 7793 using muse ifs. *Monthly Notices of the Royal Astronomical Society*, 530(1):1078–1117, 03 2024.

[9] D. A. Green. An updated catalogue of 310 galactic supernova remnants and their statistical properties, 2024.

[10] K. S. Long. Supernova remnants. In Alsabti and Murdin, editors, *Handbook of Supernovae*, pages 2005–2040. Springer, 2017.

[11] P. Musté. snr-analysis-ngc628-ngc5068. `https://github.com/Pol-M-F/snr-analysis-ngc628-ngc5068`. GitHub repository.

Identificació i caracterització de romanents de supernova en l'òptic i en raigs X

Author: Pol Musté Ferré, pmustefe25@alumnes.ub.edu
Facultat de Física, Universitat de Barcelona, Diagonal 645, 08028 Barcelona, Spain.

Advisors: Maria Kopsacheili and Konstantina Anastasopoulou

Resum: Aquest article presenta una anàlisi de múltiples longituds d'ona de romanents de supernova (SNRs) en les galàxies NGC 628 i NGC 5068, basat en les dades òptiques d'arxiu de MUSE i les observacions en raigs X de Chandra. Els candidats a SNR s'identifiquen mitjançant diagnòstics de línies d'emissió i la selecció es realitza segons criteris establerts. Els fluxos corregits per extinció permeten la derivació de lluminositats, densitats i velocitats de xoc. Utilitzant les dades òptiques, es duu a terme una comparació entre les dues galàxies per identificar qualsevol tendència. Addicionalment, s'identifiquen les contraparts en raigs X de les candidates òptiques de SNR i es presenten les seves propietats.
Paraules clau: ISM: romanents de supernova — línies: identificació — galàxies: individual: NGC 5068, NGC 628 — raigs X: general
ODSs: Educació de qualitat

Objectius de Desenvolupament Sostenible (ODSs o SDGs)

1. Fi de la es desigualtats		10. Reducció de les desigualtats	
2. Fam zero		11. Ciutats i comunitats sostenibles	
3. Salut i benestar		12. Consum i producció responsables	
4. Educació de qualitat	X	13. Acció climàtica	
5. Igualtat de gènere		14. Vida submarina	
6. Aigua neta i sanejament		15. Vida terrestre	
7. Energia neta i sostenible		16. Pau, justícia i institucions sòlides	
8. Treball digne i creixement econòmic		17. Aliança pels objectius	
9. Indústria, innovació, infraestructures			

A. Aperture Photometry Procedure

Aperture photometry was performed using a circular aperture of radius r centered at the source position (x, y), and a background annulus with inner radius $r + 1.5$ and outer radius $r + 2.5$. The total flux in the aperture is:

$$F_{\text{source}} = \sum D_i, \quad \sigma_{\text{source}} = \sqrt{\sum \sigma_i^2} \tag{A1}$$

where D_i are the pixel values and σ_i their uncertainties.

The background is estimated as the median value B of the pixels in the annulus, and its uncertainty σ_B is taken as the standard deviation of the corresponding errors taken from the error maps. The background contribution in the aperture is:

$$F_{\text{bkg}} = B \cdot A, \quad \sigma_{\text{bkg}} = \sigma_B \cdot A \tag{A2}$$

where A is the area of the aperture in pixels.

Finally, the net flux and its uncertainty are computed as:

$$F_{\text{net}} = F_{\text{source}} - F_{\text{bkg}}, \quad \sigma_{\text{net}} = \sqrt{\sigma_{\text{source}}^2 + \sigma_{\text{bkg}}^2} \tag{A3}$$

B. Diagnostic Functions for Optical SNR Classification

The following functions, proposed by [7], are used to classify optical SNRs based on emission-line ratios. A source is considered an SNR if the value of the function f is positive.

(i) For the [S II]/Hα – [N II]/Hα diagnostic:

$$\begin{aligned} f(x,y) = & -2.452xy + 0.029xy^2 + 2.244x + 0.175x^2y \\ & - 0.257x^2 - 0.043x^3 + 1.116y + 1.388y^2 \\ & - 0.217y^3 + 2.763 \end{aligned} \tag{B1}$$

where the variables are $x = \log_{10}([\text{S II}]/\text{H}\alpha)$ and $y = \log_{10}([\text{N II}]/\text{H}\alpha)$.

(ii) For the [N II]/Hα – [O III]/Hβ diagnostic:

$$f(x,y) = 0.939x + 1.0y + 0.469 \tag{B2}$$

where the variables are $x = \log_{10}([\text{N II}]/\text{H}\alpha)$ and $y = \log_{10}([\text{O III}]/\text{H}\beta)$.

(iii) For the [S II]/Hα – [O III]/Hβ diagnostic:

$$\begin{aligned} f(x,y) = & -0.781xy - 0.318xy^2 + 4.66x + 0.148x^2y - 1.821x^2 \\ & + 0.079x^3 + 4.433y - 0.479y^2 + 0.255y^3 + 3.403 \end{aligned} \tag{B3}$$

where the variables are $x = \log_{10}([\text{S II}]/\text{H}\alpha)$ and $y = \log_{10}([\text{O III}]/\text{H}\beta)$.

(iv) For the [N II]/Hα – [S II]/Hα – [O III]/Hβ diagnostic:

$$\begin{aligned} f(x,y,z) = & -2.913x^3 - 0.638x^2z + 1.568x^2y + 0.407x^2 \\ & - 0.866xz^2 - 2.264xyz + 1.508zx + 1.753xy^2 \\ & - 6.913xy + 0.001xz + 1.463z^3 - 1.325yz^2 \\ & - 2.732z^2 + 1.823y^2z - 2.697yz + 4.377z \\ & - 1.585y^3 + 0.770y^2 + 1.267y + 2.413 \end{aligned} \tag{B4}$$

where the variables are $x = \log_{10}([\text{N II}]/\text{H}\alpha)$, $y = \log_{10}([\text{S II}]/\text{H}\alpha)$ and $z = \log_{10}([\text{O III}]/\text{H}\beta)$.

In all cases, a positive value of $f(x, y)$ or $f(x, y, z)$ indicates that the source lies within the SNR classification region of the diagnostic diagram. All functions (including others not used in this work) are available at the following repository [6].

C. Color Images of NGC 628 and NGC 5068 with Identified Sources

This appendix presents color composite images of the galaxies NGC 628 and NGC 5068. The images were created using the Hα, [O III], and [S II] flux maps to highlight different emission features. All sources identified in both the optical and X-ray bands are marked.

Fig. 4 shows the color image of NGC 628 with the detected sources. Fig. 5 presents the corresponding image for NGC 5068.

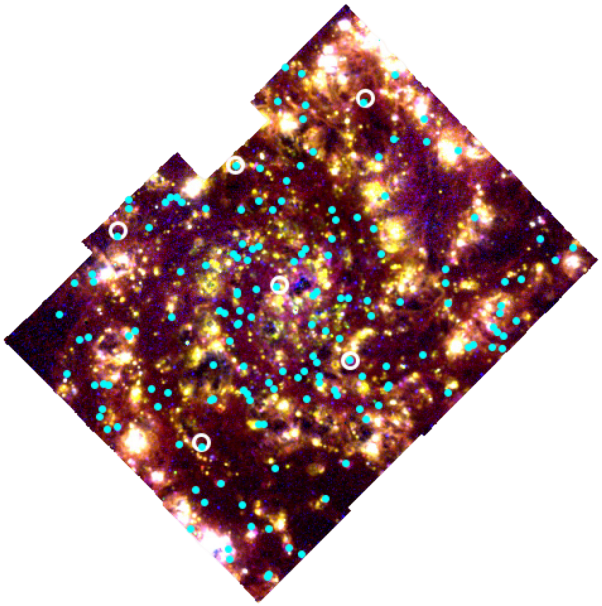

FIG. 4: Color composite image of NGC 628 created from Hα, [O III] and [S II] flux maps. All sources detected in the optical and X-ray bands are marked in cyan and white, respectively.

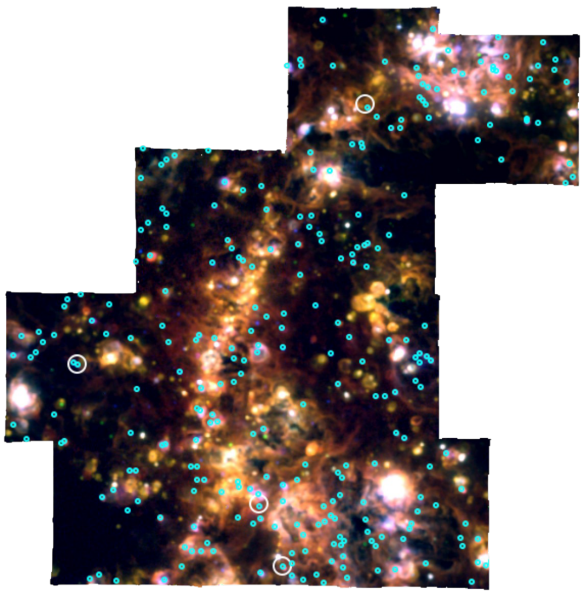

FIG. 5: Color composite image of NGC 5068 created from Hα, [O III], and [S II] flux maps. All sources detected in the optical and X-ray bands are marked in cyan and white, respectively.

D. Luminosities Histograms

The remaining histogram luminosities of Hβ, [O III], [S II] and [N II] are shown in Fig. 6:

E. Densities Histograms

For the remaining temperatures (T = 5×10^3, 3×10^4 and 5×10^4 K) the density histograms are presented in Fig. 7.

F. X-ray Source Properties

In Table IV the properties of the X-ray SNRs from NGC 628 and NGC 5068 are presented.

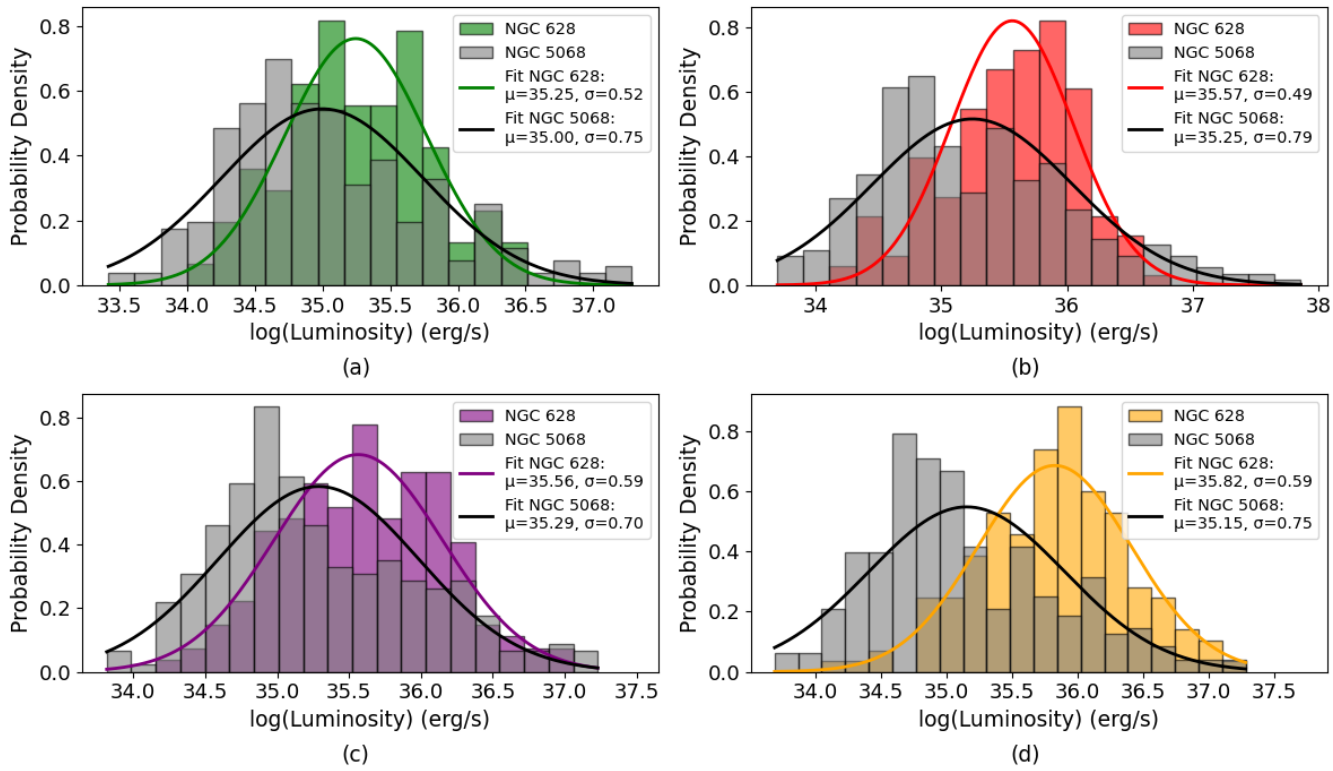

FIG. 6: Probability distributions of extinction-corrected luminosities for (a) Hβ, (b) [O III], (c) [S II] and (d) [N II] in NGC 628 and NGC 5068.

NGC 628							
RA (deg)	**Dec (deg)**	$F_{\rm abs}$ **(erg cm^{-2} s^{-1})**	$F_{\rm unabs}$ **(erg cm^{-2} s^{-1})**	$\log_{10}(L_{\rm abs})$ **(erg s^{-1})**	$\log_{10}(L_{\rm unabs})$ **(erg s^{-1})**	**S/N**	**Detected in bands**
24.183	15.799	$(5.41 \pm 2.27) \times 10^{-16}$	$(6.74 \pm 2.82) \times 10^{-16}$	36.68 ± 0.15	36.78 ± 0.15	2.39	medium, soft
24.199	15.791	$(3.69 \pm 1.85) \times 10^{-16}$	$(4.60 \pm 2.30) \times 10^{-16}$	36.52 ± 0.18	36.61 ± 0.18	2.00	medium, soft
24.177	15.784	$(1.00 \pm 0.31) \times 10^{-15}$	$(1.25 \pm 0.38) \times 10^{-15}$	36.95 ± 0.12	37.05 ± 0.12	3.28	soft
24.167	15.774	$(1.09 \pm 0.32) \times 10^{-15}$	$(1.35 \pm 0.40) \times 10^{-15}$	36.99 ± 0.11	37.08 ± 0.11	3.39	medium, soft
24.187	15.763	$(1.80 \pm 0.41) \times 10^{-15}$	$(2.25 \pm 0.52) \times 10^{-15}$	37.21 ± 0.09	37.30 ± 0.09	4.36	hard, medium, soft
NGC 5068							
RA (deg)	**Dec (deg)**	$F_{\rm abs}$ **(erg cm^{-2} s^{-1})**	$F_{\rm unabs}$ **(erg cm^{-2} s^{-1})**	$\log_{10}(L_{\rm abs})$ **(erg s^{-1})**	$\log_{10}(L_{\rm unabs})$ **(erg s^{-1})**	**S/N**	**Detected in bands**
199.724	-21.058	$(5.10 \pm 0.63) \times 10^{-16}$	$(6.35 \pm 2.15) \times 10^{-16}$	36.21 ± 0.15	36.31 ± 0.15	2.37	hard, medium, soft
199.712	-21.013	$(1.24 \pm 1.55) \times 10^{-15}$	$(1.55 \pm 3.46) \times 10^{-15}$	36.60 ± 0.11	36.69 ± 0.11	3.59	hard, medium, soft
199.746	-21.043	$(3.73 \pm 4.65) \times 10^{-14}$	$(4.65 \pm 1.82) \times 10^{-14}$	38.08 ± 0.02	38.17 ± 0.02	20.52	hard, medium, soft
199.721	-21.065	$(3.46 \pm 4.31) \times 10^{-16}$	$(4.31 \pm 1.77) \times 10^{-16}$	36.04 ± 0.18	36.14 ± 0.18	1.95	medium, soft

TABLE IV: Broad-band X-ray properties of candidate SNRs in the galaxies NGC∼628 and NGC∼5068.

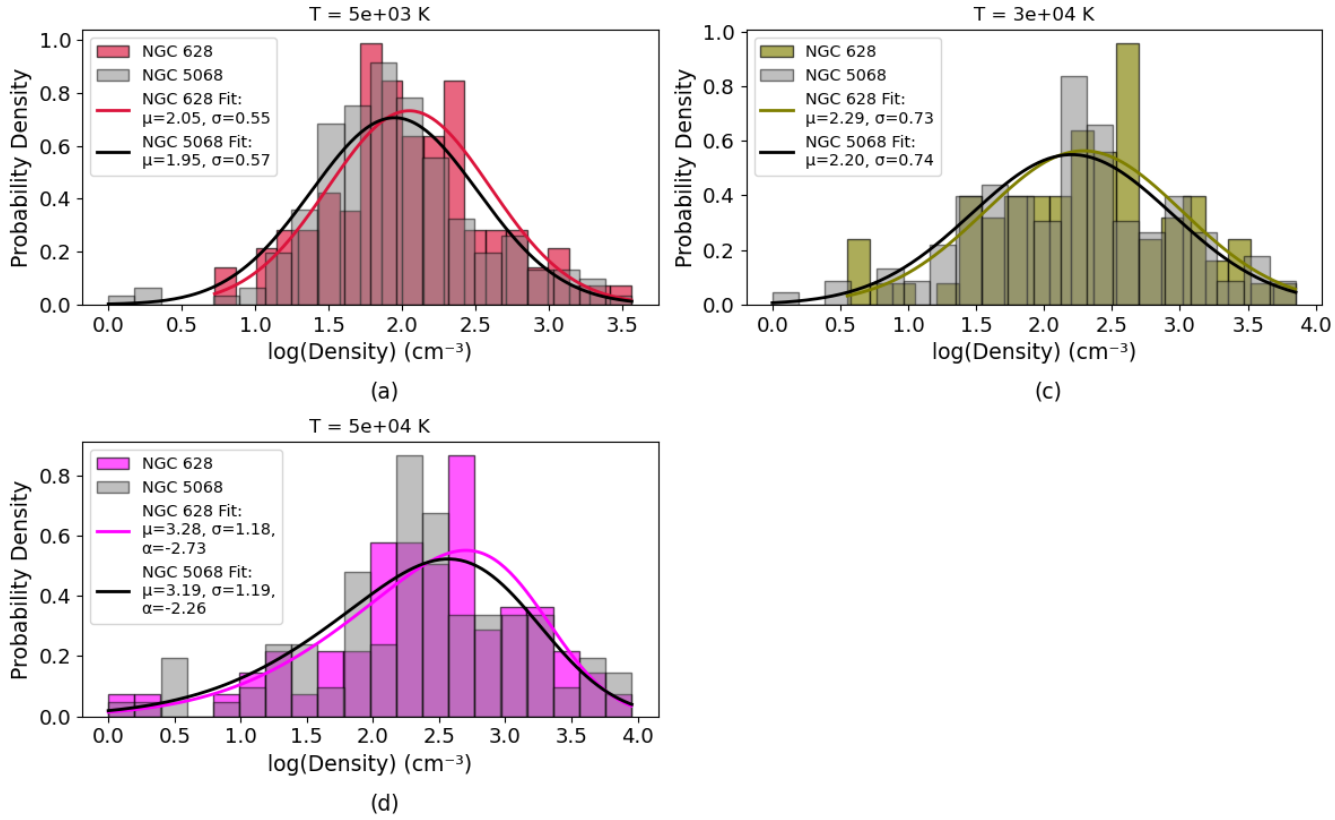

FIG. 7: Probability density functions of the estimated densities of SNRs at the temperatures of (a) 5×10^3 K, (b) 3×10^4 K and (c) 5×10^4 K in NGC 628 and NGC 5068.